All-optical measurements of background, amplitude, and timing jitters for high speed pulse trains or PRBS sequences using autocorrelation function

J. Fatome [a,*], J. Garnier [b], S. Pitois [a], M. Petit [a], G. Millot [a], M. Gay [c], B. Clouet [c], L. Bramerie [c], J.-C. Simon [c]

[a] *Institut Carnot de Bourgogne (ICB), UMR-CNRS 5209, Université de Bourgogne, 9 av. A. Savary, BP 47 870, 21078 Dijon, France*
[b] *Laboratoire de Probabilités et Modèles Aléatoires & Laboratoire Jacques-Louis Lions, Université Paris VII, 2 Place Jussieu, 75251 Paris Cedex 5, France*
[c] *ENSSAT, Plateforme PERSYST, UMR-CNRS FOTON 6082, 6 rue de Kerampont, 22300 Lannion, France*

Abstract

We present a simple method for all-optical measurements of background, amplitude, and timing jitters of ultra high speed pulse trains or PRBS sequences using the jitter dependence of the intercorrelation-peak shape. This method is numerically and experimentally demonstrated on a 42.66-Gbit/s PRBS sequence and then applied to measure the jitter growths occurring during the propagation of a 160-GHz pulse train in a classical SMF/DCF dispersion map.

© 2007 Elsevier Inc. All rights reserved.

1. Introduction

In future ultrafast telecommunication systems using optical time division multiplexing and dispersion management techniques, picosecond and even subpicosecond pulses will be transmitted through optical fibers at very high bit rates >80 Gbit/s [1–3]. Consequently, the ability to measure the quality and parameters such as extinction ratio, timing, and amplitude jitters of high speed clocks or transmitted pulse trains has become of a great interest for telecommunication engineers and transmission line designers. Unfortunately, for pulse trains beyond the bandwidth limit of electronic devices, no optical sampling oscilloscope are yet commercially available and we can assume that future devices will evolve in a very expensive trend. Consequently, checking the quality of ultrahigh speed pulse trains is still a recurring question. Frequency resolved optical gating (FROG) has been proposed a few years ago and was proved to be a powerful method to characterize such high speed pulse trains in intensity and phase even for pseudo ran-

dom bit sequences (PRBS) [4–6]. But, even though the FROG technique gives a large number of parameters (intensity and phase profiles, extinction ratio), it is generally a time consuming method (not suitable for real time monitoring) and does not permit timing and amplitude jitter measurements [6]. The optical autocorrelator is often associated to the FROG technique [6]. In contrast to the sampling oscilloscope, the time-averaging of the autocorrelation function allows the use of low-speed, high sensitivity detectors, does not require a local pulse source and can be used even on signals with closed eye diagrams [6]. It is the reason why many people, even in the telecommunication field, use the autocorrelation function to control the pulse shape [3]. But, even if the autocorrelation function has already been proved to be an efficient way to measure the timing jitter of 40-Gbit/s PRBS sequences [7] or the optical to noise ratio (OSNR) impairments at 10 Gbit/s [8], generally speaking, they do not pull all the benefits out of their measurements [3]. In this paper, we propose an extension of these methods and report an all optical technique for the simultaneous measurements of the intensity background, timing, and amplitude jitters of high speed repetition rate pulse trains or PRBS sequences. This technique is based on the distinct behavior of the auto-

---

correlation and intercorrelation peaks of the signal under test and more specifically on the timing and amplitude jitter dependences of the intercorrelation peak amplitude and width. By means of numerical simulations followed by 42.66-Gbit/s PRBS and 160-GHz experiments, we successfully demonstrate that this method can be employed for the jitter characterization of periodic or PRBS pulse trains. We believe that such a simple, all optical and relatively cheap method could find a large area of applications in the field of ultrahigh repetition rate optical signals such as high speed mode lock lasers, optical clock or differential phase shift keying (DPSK) signal characterizations.

2. Theory and simulations

The first piece of work we carried out leads to the determination of the amplitude and timing jitters of a simulated 160-GHz pulse train. First of all, the intensity autocorrelation function $A(\tau)$ of an optical signal $I(t)$ is obtained from the interaction of two time-delayed (τ) replicas of the signal under test and is defined as [6]

$$A(\tau) = \int I(t)I(t - \tau)\,dt. \qquad (1)$$

Practically, Fig. 1a shows how this optical autocorrelation function can be experimentally obtained and corresponds to the setup of our second-harmonic generation (SHG) background-free autocorrelator device used in the following experiments [4]. The two time-delayed replicas of the input signal are obtained

(a)

(b)

Fig. 1. (a) Autocorrelation experimental setup. (b) Example of a 160-GHz pulse train experimental autocorrelation function.

through a 50:50 beam splitter while the variable time delay is tuned by means of a step-motor controlled translation stage. Then, the two replicas are focused in a 2-mm-thick BBO crystal by a 5 cm focusing lens. Note that a polarization controller (PC) is also used to minimize the insertion loss of the polarizer placed at the autocorrelator input and to optimize the SHG signal. Finally, after injection in an optical fiber thanks to a micro-lens, the second harmonic autocorrelation signal is detected by means of a photo-multiplier and an oscilloscope.

Figure 1b illustrates an example of an experimental recorded 160-GHz pulse train autocorrelation function. The autocorrelation peak $A_{AC}(\tau)$ is obtained from the correlation of the signal by its nondelayed replica ($\tau \leqslant |T/2|$, T is the signal period) and this is the reason why it represents the autocorrelation of an individual pulse and that its maximum is always equal to 1 even if neighboring pulses are quite different. At the opposite, the intercorrelation peak $A_{XC}(\tau)$ ($\tau \geqslant |T/2|$) results from the correlation between neighboring pulses and is consequently dramatically sensitive to neighboring pulse differences. The method we proposed in this paper is to characterize high speed pulse trains or PRBS sequences by comparing the autocorrelation and intercorrelation peaks of the signal under test.

During its generation or propagation, essentially because of nonlinear interactions between neighboring pulses or noise, the pulse train may get amplitude and timing jitters and can be expressed assuming Gaussian pulse shape as

$$I(t) = \sum_n I_n(t - nT), \quad I_n(t) = a_n \exp\left(-\frac{(t + \tau_n)^2}{2t_0^2}\right), \qquad (2)$$

where T is the pulse train period, n is the pulse index, a_n is the amplitude jitter which is assumed to have Gaussian statistics with an average value equal to 1 and a standard deviation σ_a. τ_n is the timing jitter which is assumed to have Gaussian statistics with an average value of 0 and a standard deviation σ_t. Note that this method can be applied only if jitters are sufficiently fast to consider that pulses act individually, i.e., no difference could be observed between auto- and inter-correlation peaks if a slow jitter is applied to the pulse train. Finally, t_0 corresponds to the RMS width and related to the full-width at half maximum (FWHM) by [9]

$$\text{FWHM} = 2t_0\sqrt{2\ln(2)}. \qquad (3)$$

In absence of jitters, the autocorrelation and intercorrelation peaks of I(t) are equal and are given by

$$A_{AC}(\tau) = A_{XC}(\tau) = t_0\sqrt{\pi}\exp\left(-\frac{\tau^2}{4t_0^2}\right). \qquad (4)$$

Figure 2 shows an illustration of the intensity profile of an ideal 160-GHz pulse train as well as its autocorrelation function, respectively Figs. 2a and 2b, dashed line. At the same time, solid lines represent this pulse train numerically damaged by adding timing (0.4 ps) and amplitude (20%) jitters. The number of periods is chosen to be sufficiently large (2^{12}) in order to have an efficient statistical distribution. Density functions of timing and amplitude jitters are plotted in Figs. 2c and 2d and show pretty well Gaussian shapes with an average of 0 ps for the arrival time and an average of 1 for the peak intensity.
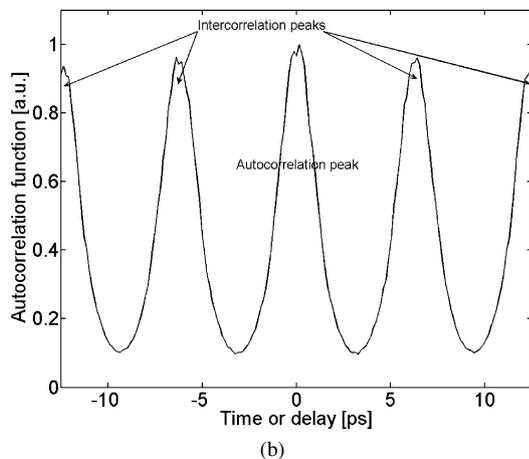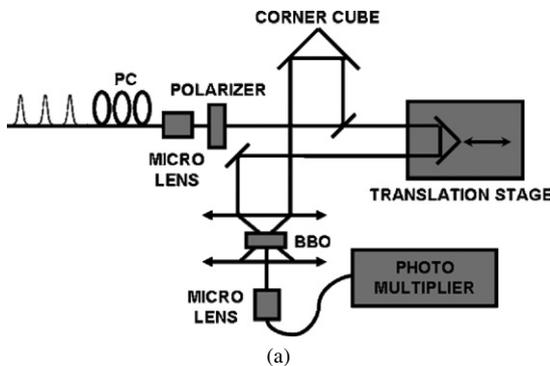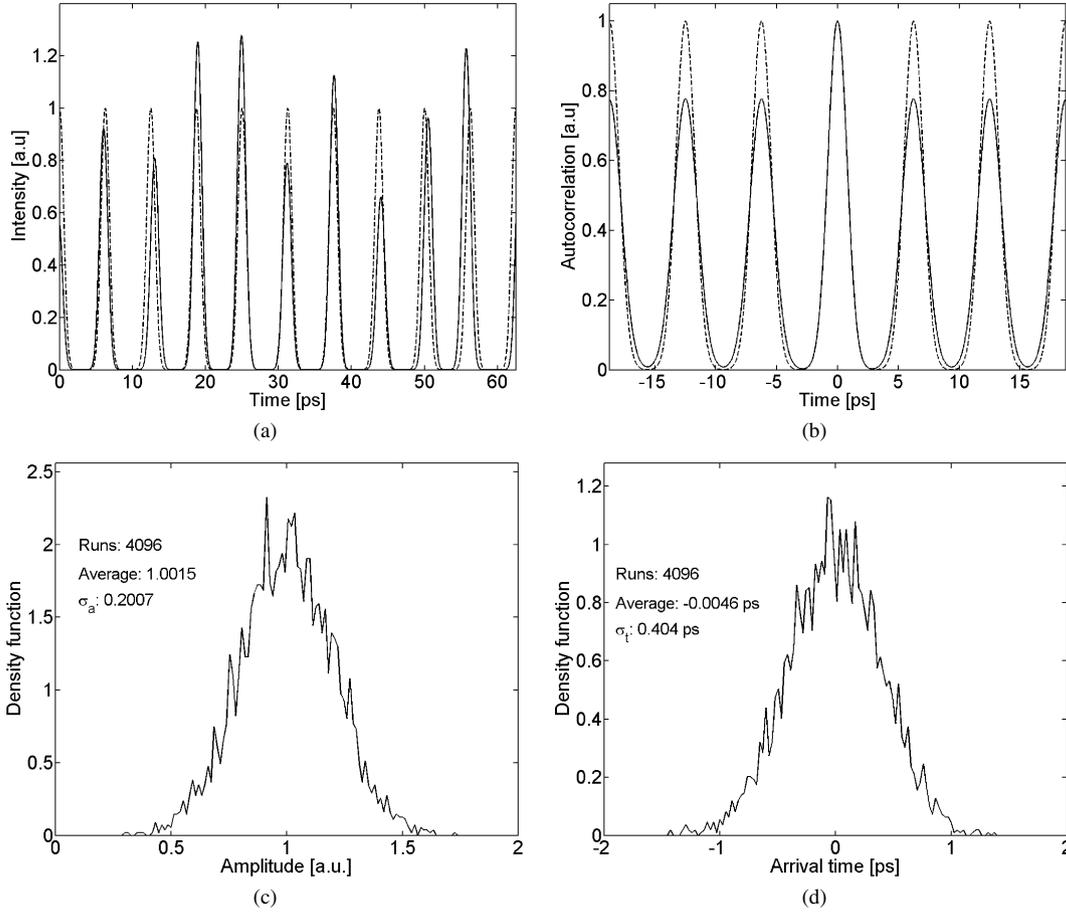
Fig. 2. (a) Initial 160-GHz pulse train (dashed line) and degraded with timing (0.4 ps) and amplitude (20%) jitters (solid line). (b) Autocorrelation function of initial (dashed line) and degraded pulse train. (c) Probability density of the amplitude jitter. (d) Probability density of the timing jitter.

By comparing the initial (dashed line) and degraded (solid line) autocorrelation functions of the 160-GHz pulse train in Fig. 2b, we can clearly observe that the presence of amplitude and timing jitters is characterized by a dramatic attenuation and broadening of the intercorrelation peaks, translating the differences between neighboring pulses. This behavior could be greatly observed in Ref. [3] where the autocorrelation function of an 85-Gbit/s DPSK signal has been recorded until 4320 km.

In presence of timing and amplitude jitters, the autocorrelation and intercorrelation peaks (respectively A_{AC} and A_{XC}) can be obtained by injecting expression (2) in Eq. (1) and are then given by

$$A_{AC}(\tau) = \langle a_0^2 \rangle \left\langle \int \exp\left(-\frac{t^2}{2t_0^2} - \frac{(\tau - t)^2}{2t_0^2}\right) dt \right\rangle,$$

$$A_{AC}(\tau) = \langle a_0^2 \rangle \sqrt{\pi} t_0 \exp\left(-\frac{\tau^2}{4t_0^2}\right),$$

$$A_{XC}(\tau) = \langle a_0 a_1 \rangle \left\langle \int \exp\left(-\frac{t^2}{2t_0^2} - \frac{(\tau - t - \Delta\Gamma)^2}{2t_0^2}\right) dt \right\rangle,$$

$$A_{XC}(\tau) = \langle a_0 a_1 \rangle \sqrt{\pi} t_0 \left\langle \exp\left(-\frac{(\tau - \Delta\Gamma)^2}{2t_0^2}\right) \right\rangle, \tag{5}$$

where $\Delta\Gamma = \tau_0 - \tau_1$, τ_0 and τ_1 (respectively a_0 and a_1) are the timing jitters (respectively amplitude jitters) for two neighbor-

ing pulses, and $\langle - \rangle$ stands for statistical averaging. Assuming independent Gaussian statistics for the timing and amplitude jitters, the autocorrelation and intercorrelation peaks have now the following form:

$$A_{AC}(\tau) = \left(1 + \sigma_a^2\right) \sqrt{\pi} t_0 \exp\left(-\frac{\tau^2}{4t_0^2}\right),$$

$$A_{XC}(\tau) = \frac{\sqrt{\pi} t_0}{\sqrt{1 + \sigma_t^2/t_0^2}} \exp\left(-\frac{\tau^2}{4t_0^2} \frac{1}{1 + \sigma_t^2/t_0^2}\right). \tag{6}$$

From this analysis, we can express the timing and amplitude jitters in terms of the full-width at half maximum FWHM_{AC} and FWHM_{XC} of the autocorrelation and intercorrelation peaks, and in terms of their amplitudes P_{AC} and P_{XC}:

$$\sigma_t = \frac{1}{4\sqrt{\ln 2}} \left[\text{FWHM}_{XC}^2 - \text{FWHM}_{AC}^2\right]^{1/2},$$

$$\sigma_a = \left[\frac{P_{AC}}{P_{XC}} \left(1 + \frac{\sigma_t^2}{t_{0\text{mes}}^2}\right)^{-1/2} - 1\right]^{1/2}, \tag{7}$$

where $t_{0\text{mes}}$ is given by $t_{0\text{mes}} = \text{FWHM}_{AC}/(4\sqrt{\ln 2})$.

The expression for the timing jitter is consistent with the one derived in Ref. [7]. Here we show that it holds true even in the presence of amplitude jitter. In other words, because broadening of the intercorrelation peak was only due to the timing jitter,

Table 1

Comparison between the simulated and retrieved jitters of a 160-GHz pulse train

	FWHM (ps)	Peak		σ_t (ps)	σ_a
A_{AC}	1.81	1	Simulation	0.40	0.20
A_{XC}	2.25	0.78	Retrieved	0.40	0.19

its measurement with the correlation setup is not sensitive to the amplitude jitter. Consequently, the amplitude and timing jitters can now be extracted simply from the experimental measurements of the autocorrelation and intercorrelation peak FWHMs and amplitudes.

Another interesting result is that we can compute the errors on the measured values of σ_t and σ_a by performing a linear stability analysis of expressions (7). If Δt, respectively ΔP, represents the temporal resolution, respectively the amplitude resolution, of the correlation setup, we obtain

$$\Delta \sigma_t = \frac{1}{4\sqrt{\ln 2}} \left[\frac{\text{FWHM}_{XC}^2 + \text{FWHM}_{AC}^2}{\text{FWHM}_{XC}^2 - \text{FWHM}_{AC}^2} \right]^{1/2} \Delta t,$$

$$\Delta \sigma_a = \sigma_a \left[\frac{\Delta P^2}{P_{AC}^2} + \frac{\Delta P^2}{P_{XC}^2} + \frac{\Delta t^2}{\text{FWHM}_{AC}^2} + \frac{\Delta t^2}{\text{FWHM}_{XC}^2} \right]^{1/2}. \quad (8)$$

Note that the timing jitter measurement accuracy is inversely proportional to the square root of the timing jitter, which shows that this method has rather poor resolution when the timing jitter is small. At the opposite, the amplitude jitter measurement accuracy is, roughly speaking, proportional to the jitter itself, which shows that it is efficient even when the jitters are small.

For example, Table 1 gives a comparison between the simulated jitters defined as the standard deviation of the density functions plotted in Figs. 2c and 2d and those retrieved from Eq. (7) by means of FWHMs and amplitudes of autocorrelation and intercorrelation peaks. We can clearly see an excellent agreement between the simulated and calculated results, proving the reliability of the method.

We would like to stress that this method is unlimited in frequency and thus could be used to characterize pulse sources with high repetition rates beyond the electronic sampling oscilloscope limitation. Recording the autocorrelation function of DPSK format during the propagation, as in Ref. [3], could now become a powerful measurement which is presently underestimated in the telecommunication field.

2.1. PRBS pulse train

This method can be applied to a pseudo-random bit sequence (PRBS) as well, providing that the length of the sequence is sufficiently large to ensure a fair statistical distribution between "0" and "1." In this case, the maximum of the initial intercorrelation peak becomes R (ratio of "1" in the sequence) in contrast to 1 in the periodic case. Consequently, in the PRBS case, the expression of the timing jitter in Eq. (7) is still valid while that of the amplitude jitter becomes

$$\sigma_a = \left[\frac{R}{P_{XC}} \left(1 + \frac{\sigma_t^2}{t_{0mes}^2} \right)^{-1/2} - 1 \right]^{1/2}. \quad (9)$$
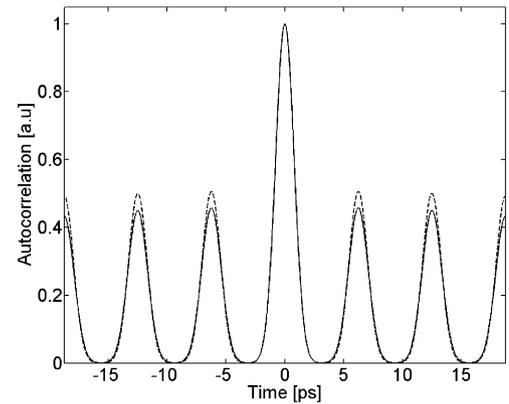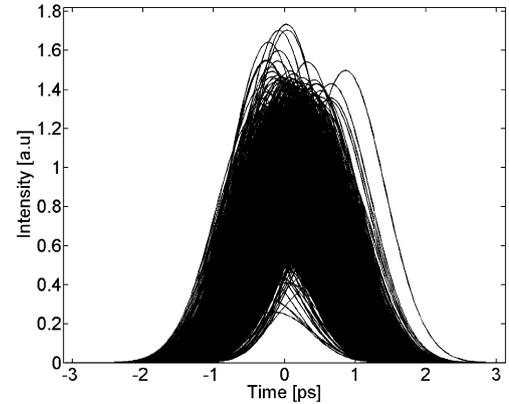

(a)

(b)

Fig. 3. (a) Eye diagram of the 160-Gbit/s PRBS sequence degraded with timing (0.2 ps) and amplitude (20%) jitters. (b) Autocorrelation function of the initial (dashed line) and degraded 160-Gbit/s PRBS sequence.

Table 2

Comparison between the simulated and retrieved jitters of a 160-Gbit/s PRBS sequence

	σ_t (ps)	σ_a
Simulation	0.20	0.20
Retrieved	0.20	0.19

Note that in a true PRBS sequence, the number of "0" is equal to the number of "1" and $R = 0.5$.

Figure 3a shows the eye diagram of a 160-Gbit/s PRBS sequence damaged by timing (0.2 ps) and amplitude (20%) jitters. Figure 3b represents the autocorrelation function of this initial (dashed line) and degraded (solid line) 160-Gbit/s sequence.

By means of Eqs. (7) and (9), one can calculate the timing and amplitude jitters of the sequence. Table 2 sums up the results. As in the periodic case, we can see an excellent agreement between simulated and retrieved jitters.

2.2. Pulse train with background

Because of the intrinsic features of pulse sources (fiber ring lasers, nonlinear optical loop mirrors, optical modulators), or simply because of nonlinear interactions with noise or neighboring pulses in optical fiber, we have to consider the case where pulses are degraded or raised on an intensity background. As a result, the model for the nth pulse intensity becomes

$$I_n(t) = f_d + (1 - f_d)a_n \exp\left(-\frac{(t + \tau_n)^2}{2t_0^2}\right), \tag{10}$$

where f_d is the intensity background.

In the general case ($R \neq 1$), the autocorrelation peak of $I(t)$ is now given by

$$
\begin{aligned}
A_{AC}(\tau) = &\left(Tf_d^2 + 2f_d(1 - f_d)\sqrt{2\pi}t_0 + (1 - f_d)^2\sqrt{\pi}t_0\right. \\
&\times \left[\exp\left(-\frac{\tau^2}{4t_0^2}\right) + R\exp\left(-\frac{(T - \tau)^2}{4t_0^2}\right)\right]\right) \\
&\times \left(Tf_d^2 + 2f_d(1 - f_d)\sqrt{2\pi}t_0 + (1 - f_d)^2\sqrt{\pi}t_0\right. \\
&\times \left[1 + R\exp\left(-\frac{T^2}{4t_0^2}\right)\right]\right)^{-1},
\end{aligned}
\tag{11}
$$

where T is the pulse train period.

The minimum of the autocorrelation function F_d is approximately reached at

$$\tau_{min} = \pm\frac{T}{2}\left(1 - \frac{4t_0^2}{T^2}\ln R\right). \tag{12}$$

Note that $\tau_{min} = \pm T/2$ in the periodic case ($R = 1$).

The value of F_d is then given by

$$
\begin{aligned}
F_d = &\left(Tf_d^2 + 2f_d(1 - f_d)\sqrt{2\pi}t_0\right. \\
&+ 2\sqrt{R}(1 - f_d)^2\sqrt{\pi}t_0\exp\left(-\frac{T^2}{16t_0^2}\right)\right) \\
&\times \left(Tf_d^2 + 2f_d(1 - f_d)\sqrt{2\pi}t_0\right. \\
&+ (1 - f_d)^2\sqrt{\pi}t_0\left[1 + R\exp\left(-\frac{T^2}{4t_0^2}\right)\right]\right)^{-1}.
\end{aligned}
\tag{13}
$$

Measuring F_d on the experimental autocorrelation function, we can get f_d by solving a quadratic equation. If F_d is small, then the solution can be expanded as

$$f_d = \frac{F_d - 2\sqrt{R}\exp(-T^2/16t_{0mes}^2)}{2\sqrt{2} - 4\sqrt{2R}\exp(-T^2/16t_{0mes}^2)} \approx \frac{F_d}{2\sqrt{2}}, \tag{14}$$

where the last expression is obtained assuming T larger than $4t_0$ (well separated pulses).

Figure 4a shows the eye diagram of a 160-GHz pulse train with an intensity background of 4% and damaged by a timing (0.2 ps) and amplitude (20%) jitters. Figure 4b represents the autocorrelation function of the initial (dashed line) and degraded (solid line) pulse train.

As in Fig. 2b, we can see that the intercorrelation peak is dramatically reduced and broadened due to the presence of amplitude and timing jitters. By removing the contribution of neighboring pulse overlapping and by supposing that timing jitter does not participate to the autocorrelation background, that
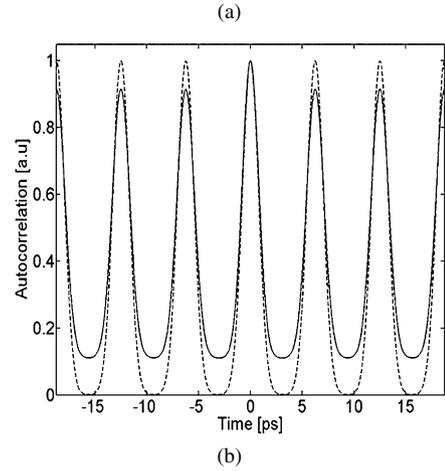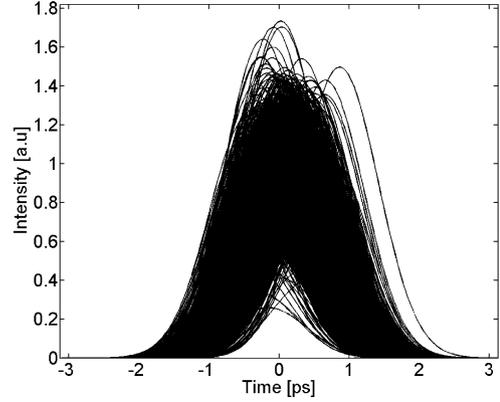

(a)

(b)

Fig. 4. (a) Eye diagram of the 160-GHz pulse train with a 4% intensity background and degraded with timing (0.2 ps) and amplitude (20%) jitters. (b) Autocorrelation function of the initial (dashed line) and degraded pulse train.

Table 3
Comparison between the simulated and retrieved jitters of a 160-GHz pulse train in presence of an intensity background

	Background	σ_t (ps)	σ_a
Simulation	0.04	0.40	0.20
Retrieved	0.04	0.40	0.19

means that timing jitter does not exceed 10% of the bit slot, the timing jitter could be also evaluated thanks to Eq. (7) by calculating the FWHMs at

$$\frac{1}{2}[P_k + F_d], \tag{15}$$

where P_k is the inter- or autocorrelation peak and F_d the measured autocorrelation background.

Under the same assumptions, the decrease of the intercorrelation peak due to the jitters is now obtained by the following expression:

$$\frac{P_{AC} - F_d}{P_{XC} - F_d} = \left(1 + \sigma_a^2\right)\left(1 + \frac{\sigma_t^2}{t_{0mes}^2}\right)^{1/2}. \tag{16}$$

For example, Table 3 gives the simulated and calculated jitters and background of the pulse train plotted in Fig. 4a. Thanks to Eqs. (7) and (14)–(16), we have successfully derived all the desired features of the pulse train from its autocorrelation function.
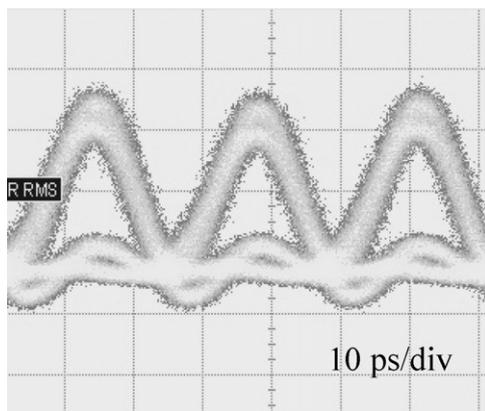
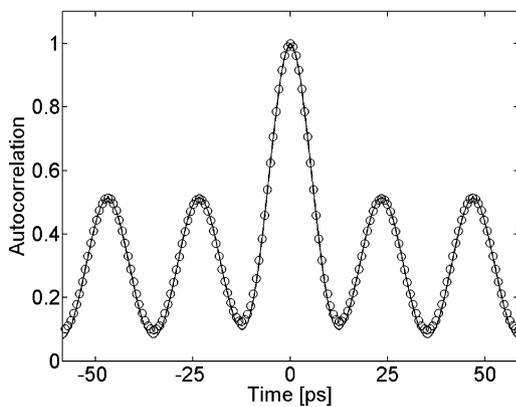## 3. Experimental results

3.1. 42.66-Gbit/s results

The first series of experiments were carried out on the technological platform PERSYST (platform for test and research on optical telecommunication system) in Lannion, France, (persyst@persyst.fr). The purpose is to characterize in the time domain a RZ 42.66-Gbit/s PRBS sequence by means of a 50-GHz optical sampling oscilloscope and thanks to the second-harmonic generation background-free optical autocorrelator described in Fig. 1a as well. Figure 5 shows the experimental setup. The signal is coded thanks to a LiNbO$_3$ modulator driven by a $2^{15} - 1$ PRBS sequence in NRZ format at 42.64 Gbit/s, generated by electrical multiplexing of 4 trains at 10.66 Gbit/s. The RZ 33% optical signal is obtained thanks to a LiNbO$_3$ modulator driven by a 21.3 GHz sinusoidal clock. Then, the sequence is injected into 100 km of nonzero dispersion shifted fiber (NZDSF, $D = 4$ ps/nm/km). Chromatic dispersion was compensated with dispersion compensating fiber (DCF) and amplification is ensured by erbium-doped fiber amplifiers (EDFA). The 42.66-Gbit/s PRBS sequence was finally characterized at the receiver by a 50-GHz optical sampling oscilloscope and by the optical autocorrelator.

We first characterized the PRBS sequence in a back-to-back configuration. Figure 6a represents the corresponding eye diagram. The timing jitter was evaluated at 1 ps by the sampling oscilloscope (corresponding to the resolution limit of the equipment). Thanks to the experimental autocorrelation function, plotted in Fig. 6b (solid line), and to Eq. (7), we have calculated a timing jitter of 0.96 ps ($\pm 2\%$, $\Delta t = 10^{-2}$ ps) which is in good agreement with the first oscilloscope measurement. In both cases, the amplitude jitters were found negligible. Moreover, we have also plotted in Fig. 6b (circles), a simulated autocorrelation function of the 42.66-Gbit/s PRBS sequence calculated from the experimental features (FWHM, jitters, background). The excellent agreement between the two different curves stresses the accuracy of the method.

Figures 7a and 7b show the experimental results obtained after 100 km of propagation. The NZDSF input power was fixed to 10 dB m in order to exacerbate the nonlinear effects so as to speed up the timing jitter creation. The timing jitter was measured to 2.5 ps by means of the sampling oscilloscope (Fig. 7a) and to 2.22 ps ($\pm 1\%$, $\Delta t = 10^{-2}$ ps) through the autocorrelation method (Fig. 7b, solid line). No significant decrease of the intercorrelation peak compared to the back-to-back mea-

Fig. 5. 42.66-Gbit/s transmission experiment, optical band pass filter (OBPF).
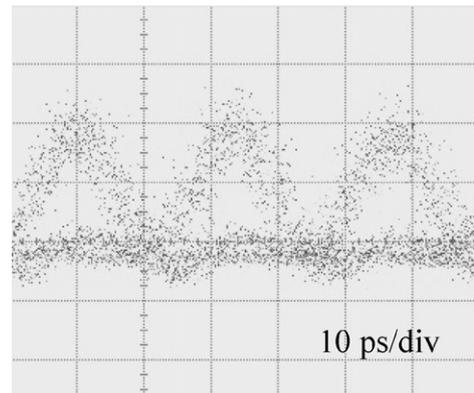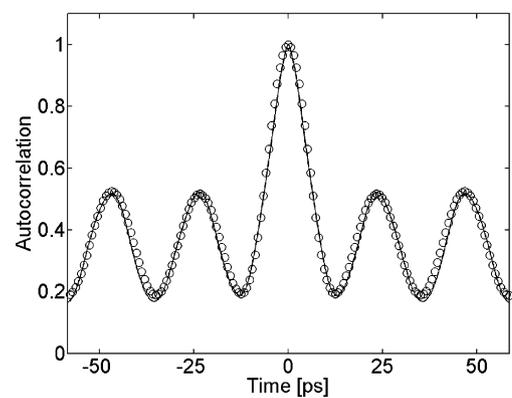

(a)

(b)

Fig. 6. (a) Eye diagram of the initial 42.66-Gbit/s PRBS sequence. (b) Corresponding autocorrelation function: experimental (solid line) and simulated (circles).

(a)

(b)

Fig. 7. (a) Eye diagram of the 42.66-Gbit/s PRBS sequence after 100 km of propagation. (b) Corresponding autocorrelation function: experimental (solid line) and simulated (circles).

surement was observed after 100 km, indicating that no amplitude jitter was generated during the propagation, which is in good agreement with the oscilloscope conclusions. Finally, on Fig. 7b, we observe a good agreement between the experimental autocorrelation function (solid line) and that simulated from the calculated features (circles), proving the reliability of the measurement.

3.2. 160-GHz results

The second series of measurements leads to the determination of the intensity background, timing and amplitude jitters of a 160-GHz pulse train during its propagation in a classical 100-km SMF/DCF recirculating loop setup. The experimental setup is shown in Fig. 8a. A high quality 160-GHz Gaussian pulse train, generated by multiple four wave mixing in a 1 km-long NZDSF [10] is injected into a 100-km-long recirculating loop setup. The dispersion map is a symmetric map [11] made of 2 spans of 50 km of SMF fiber ($D = 17$ ps/km nm, $S = 0.056$ ps/km nm^2) separated by a dispersion compensating fiber (DCF) module which compensates for 99% of the total second- and third-order chromatic dispersion of the line. Two erbium-doped fiber amplifiers (EDFA) are used to compensate for the total losses of the line while a 1.8-THz optical band pass filter (OBPF) is inserted to avoid the accumulation of noise into the loop. The output signal is finally characterized by our background-free second-harmonic generation autocorrelator described in Fig 1a.

By supposing that pulses keep a Gaussian shape during their propagation but develop a growing intensity background and by using expressions (7) and (14)–(16), we derived the FWHMs, the intensity backgrounds, the timing and amplitude jitters of the 160-GHz pulse train at 100, 400, 800, 1100, 1500, and 2000 km which experimental autocorrelation functions are plotted in Fig. 8b. Figure 9a shows the measured FWHMs and the calculated intensity backgrounds. We can observe that after an initial broadening, the pulse width stabilizes and remains constant during the propagation, indicating that the dispersion management is finely tuned. The intensity background increases during the whole propagation, indicating that strong nonlinear interactions occurred between neighboring pulses and noise and thus limited the propagation distance. Figure 9b shows the calculated timing σ_t and amplitude σ_a jitters as a function of propagation distance. We can notice that the 2 jitters dramatically increase to reach at 2000 km nearly the third of the pulse width for the timing jitter and the entire pulse peak for the amplitude jitter. Note that the error bars on Fig. 9b are calculated by means of expressions (8). Figure 9c shows the measured autocorrelation function at 800 km (solid line) and that simulated (circles) from the measured features (FWHM=1.44 ps, intensity background of 6%, $\sigma_t = 0.17$ ps and $\sigma_a = 27$%). We can observe that we found an excellent agreement between the two different curves indicating the reliability of our technique. Finally, for illustration, Fig. 9d shows the intensity profile of the 160-GHz pulse train corresponding to the simulated 800 km autocorrelation function plotted in circles in Fig. 9c. We can notice that the level of the amplitude jitter evolves in a dramatic behavior for a telecommunication system.

4. Conclusion

In this paper, we have reported a simple and all-optical method for the simultaneous measurements of the intensity background, timing, and amplitude jitters of high repetition rate pulse trains and PRBS sequences. This technique is based on the recording of the experimental optical autocorrelation function of the pulse train under test and on the timing and amplitude jitter dependences of the intercorrelation peak amplitude and width. We have derived simple expressions of the jitters as a function of the FWHMs and amplitudes of the autocorrelation and intercorrelation peaks both in the periodic and PRBS case. We have also completed the analysis by computing the errors on the measurements and by deriving an expression for the intensity background. Through numerical simulations, we have successfully demonstrated that this method could be employed for the characterization of PRBS or periodic high speed pulse trains. Then, we have experimentally demonstrated the reliability of our technique by successfully computing the timing jitter of a 42.66-Gbit/s PRBS RZ sequence. Finally, we applied our method to the characterization of a 160-GHz pulse train during its propagation in a classical 100-km SMF/DCF system
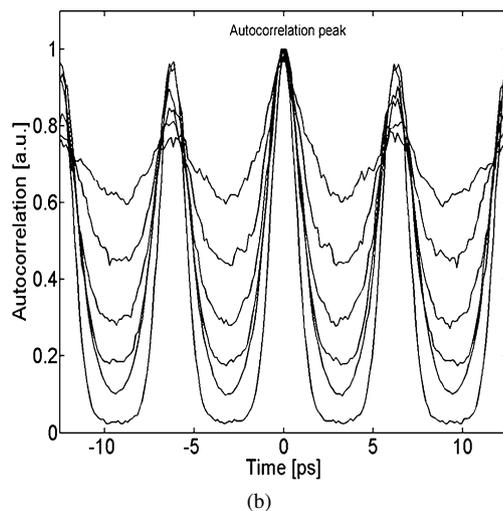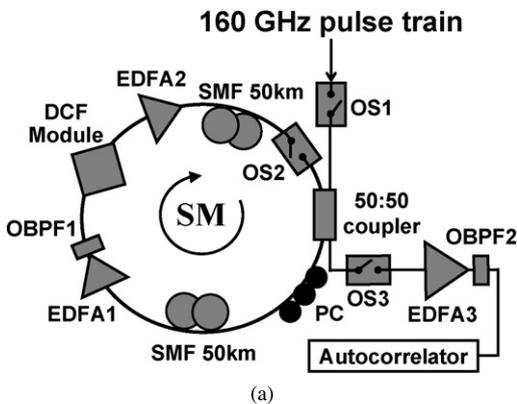

Fig. 8. (a) Experimental setup, optical switch (OS), polarization controller (PC). (b) Autocorrelation functions of the 160-GHz pulse train at (bottom to top) 100, 400, 800, 1100, 1500 and 2000 km.
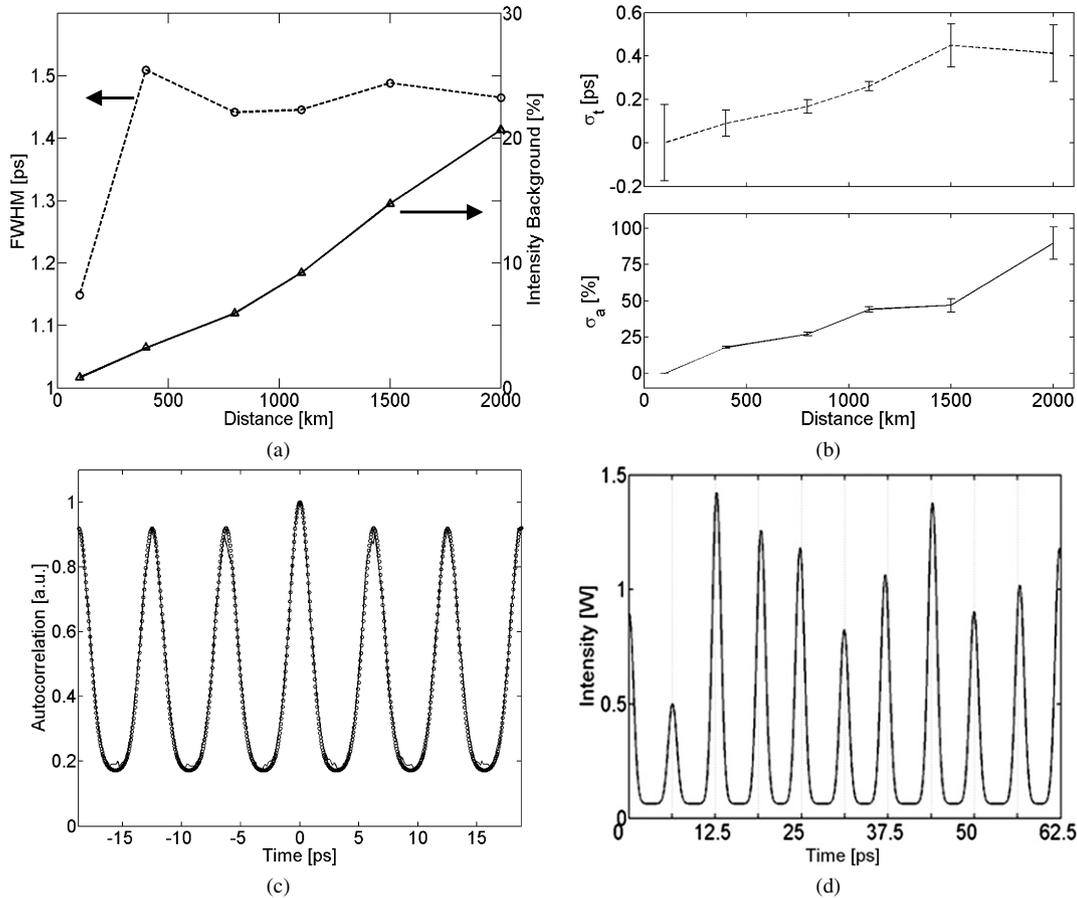
Fig. 9. (a) Measurements from experimental autocorrelation functions of FWHM (circles) and intensity background (triangle) of the 160-GHz pulse train as a function of propagation distance. (b) Measurements from experimental autocorrelation functions of amplitude σ_a (bottom) and timing jitters σ_t (top) as a function of propagation distance. (c) Autocorrelation function of the 160-GHz pulse train: recorded at 800 km (solid line) and simulated from calculated features (circles). (d) Corresponding intensity profile of the autocorrelation function simulated in (c).

and successfully derived the different features of the pulse train as a function of propagation distance (FWHM, intensity background, timing, and amplitude jitters). The main limitations of our method is that the measurement is under the assumption that pulses have a Gaussian shape, that jitters are sufficiently fast to consider that any bit acts individually, that the bandwidth of the autocorrelator (typically >THz) is sufficiently large toward the pulse train repetition rate and that in the case of an intensity background, timing jitter does not participate to the autocorrelation background. In conclusion, we believe that such a simple, relatively cheap and all-optical method could find a large area of applications in the ultrahigh speed optical field; for example: characterizing fiber ring lasers, high speed DPSK signals or high speed optical sources and clocks.

References

[1] H.G. Weber, S. Ferber, M. Kroh, C. Schmidt-Langhorst, R. Ludwig, V. Marembert, C. Boerner, F. Futami, S. Watanabe, C. Schubert, Single channel 1.28 and 2.56 Tbit/s DQPSK transmission, ECOC'05, Glasgow, 2005, Post Deadline Paper Th 4.1.2.

[2] A.H. Gnauck, G. Raybon, P.G. Bernasconi, J. Leuthold, C.R. Doerr, L.W. Stulz, 1-Tb/s (6 × 170.6 Gb/s) transmission over 2000-km NZDF using OTDM and RZ-DPSK format, IEEE Photon. Technol. Lett. 15 (11) (2003) 1618–1620.

[3] S. Weisser, S. Ferber, L. Raddatz, R. Ludwig, A. Benz, C. Boerner, H.G. Weber, Single- and alternating polarization 170-Gbit/s transmission up to 4000 km using dispersion-managed fiber and all-Raman amplification, IEEE Photon. Technol. Lett. 18 (12) (2006) 1320–1322.

[4] J. Fatome, S. Pitois, G. Millot, Sensitivity of SHG-FROG for the characterization of ultrahigh-repetition-rate telecommunication laser sources, Opt. Fiber Technol. 10 (2004) 73–78.

[5] P. Grelu, F. Gutty, G. Millot, Pseudo-random pulse sequence characterization with frequency-resolved optical gating, IEEE Photon. Technol. Lett. 14 (5) (2002) 672–674.

[6] R. Trebino, Frequency-Resolved Optical Gating: The Measurement of Ultrashort Laser Pulses, Kluwer, Boston, 2000.

[7] J. Dörring, G.B. Tudury, A. Lenihan, G.M. Carter, Y.J. Chen, All-optical timing jitter measurements on 40 Gbit/s pseudorandom RZ data after long-haul transmission in dispersion-managed soliton system, Electron. Lett. 38 (14) (2002) 727–729.

[8] M. Dinu, D.C. Kilper, H.R. Stuart, Characterization of signal quality using data stream optical autocorrelation, CLEO'04, San Francisco, 2004, Paper CThLL3.

[9] G.P. Agrawal, Nonlinear Fiber Optics, third ed., Academic Press, New York, 2001.

[10] S. Pitois, J. Fatome, G. Millot, Generation of a 160-GHz transform-limited pedestal-free pulse train through multiwave mixing compression of a dual-frequency beat signal, Opt. Lett. 27 (19) (2002) 1729–1731.

[11] J. Fatome, S. Pitois, P. Tchofo-Dinda, G. Millot, E.L. Rouzic, B. Cuenot, E. Pincemin, S. Gosselin, Effectiveness of fiber lines with symmetric dispersion swing for 160-Gb/s terrestrial transmission systems, IEEE Photon. Technol. Lett. 16 (10) (2004) 2365–2367.